Surface-mode enhanced photonic-crystal nano-imaging observed by a scanning near-field optical microscope

Qiming Zhang, Xiangping Li, and Min Gu[a)]
Faculty of Engineering and Industrial Sciences, Centre for Micro-Photonics, Swinburne University of Technology, Hawthorn, VIC 3122, Australia

(Received 1 May 2013; accepted 18 July 2013; published online 30 July 2013)

In this paper, we experimentally demonstrate the sub-wavelength loss-less nano-imaging effect achieved by the surface-mode coupling in a negative refraction silicon photonic crystal at a wavelength of 1100 nm. The surface mode and nano-imaging effect of the photonic crystal are experimentally studied with a scanning near-field optical microscope. The thickness and the wavelength dependence of the full width at half maximum of the focal spot reveal a direct evidence of the surface-mode enhanced nano-imaging effect, which is consistent with the simulation. As a consequence, a focal spot with a lateral resolution of $\lambda/3$ at the predicted wavelength has been achieved. © *2013 AIP Publishing LLC*. [http://dx.doi.org/10.1063/1.4817318]

Owing to its capability to break the diffraction limit, a flat lens composed of negative refractive index (NRI) materials proposed by Pendry[1] has attracted intense research efforts. Such a kind of structure can not only focus the propagating wave but also recover the evanescent waves which contain the fine details of the object by supporting the surface plasmon polaritons (SPPs).[2] Despite the fact that SPPs enhanced nano-imaging in the nearfield beyond the diffraction limit has been demonstrated in metamaterials and metallic structures,[3,4] the performance of the reported metal based NRI materials is limited by the high loss associated with the intrinsic absorption of metals at optical frequencies. On the contrary, photonic crystals composed of low loss dielectric materials are heralded as good candidates with effective NRI at optical frequencies from the visible to the near infrared.[5–7] However, nano-imaging beyond the diffraction limit has never been achieved in the photonic crystal slab with negative refraction properties due to the lack of supporting of high spatial-frequency components such as SPPs to recover the evanescent wave.[8–10] On the other hand, it has been known that photonic crystals can support surface-mode propagating along the surface of the photonic crystal due to the symmetry broken at the surface between photonic crystal and the background material.[11] It has been predicted that the surface mode can be used to support and recover the evanescent wave of the object by engineering the interface of the photonic crystal.[12] Coupling the surface mode to achieve the nano-imaging effect is yet to be demonstrated.

In this paper, we reported on the experimental demonstration of the nano-imaging by the surface-mode coupling in a negative refraction photonic crystal. The surface-mode enhanced nano-imaging effect of the photonic crystal was studied experimentally by a scanning near-field optical microscope (SNOM) with a single or double excitation sources. The lateral full width at half maximum (FWHM) of the focal spot reached minima at the minimum thickness of the photonic crystal slab and at the wavelength exhibiting the strongest surface-mode coupling. Our result shows that a $\lambda/3$-resolution capability can be achieved by a photonic crystal slab fabricated on a silicon on insulator (SOI) wafer at the optical wavelength of 1100 nm.

The photonic crystal slab was fabricated on a commercial SOI wafer (Soitec). The thicknesses of the Si and SiO_2 layers are 0.26 and 1 μm, respectively. A pattern was formed on a PMMA layer coated on top of the wafer by E-beam lithography (EBPG 5000, Vistec). Then the pattern was transferred to the chromium layer by the lift-off process. The chromium layer served as a hard mask for the reactive ion etching of the silicon layer with C_4F_8 and SF_6 (ICP 380, Oxford). The high etching selectivity between chromium and silicon guarantees that the pattern transfers correctly to the silicon layer after etching.

The resulting structure is shown in Fig. 1(a). The two-dimensional photonic crystal is composed of square-lattice air holes with a lattice constant $a = 230$ nm and a radius $r = 70$ nm. The interface between the air and the photonic crystal slab is along the ΓM direction. The structures of the input and output interface are identical to support the same surface mode. The photonic crystal is designed to work at the transverse magnetic (TM) polarization. A single-mode silicon waveguide with a width of 200 nm is fabricated 100 nm away with respect to the input interface and the output light is employed as the point source for excitation. The width of the photonic crystal slab is 20 periods. While the thickness of the photonic crystal slab is changed in the experiment and simulation, the separation between the photonic crystal slab and the point source is fixed. The structures were characterized with a SNOM (Solver, NT-MDT). To confirm the negative refraction, a thick slab of the photonic crystal consisting of 11 layers was measured. A 4 μm-wide silicon waveguide was fabricated to guide the incident laser beam. The incident angle is 45°. The near-field image in Fig. 1(b) shows the beam refracted negatively at the interface of the photonic crystal and the air at the wavelength of 1100 nm.

To confirm the excitation of surface mode, we scanned the dotted region outside the excitation source in Fig. 1(a) to

[a)]Author to whom correspondence should be addressed. Electronic mail: mgu@swin.edu.au

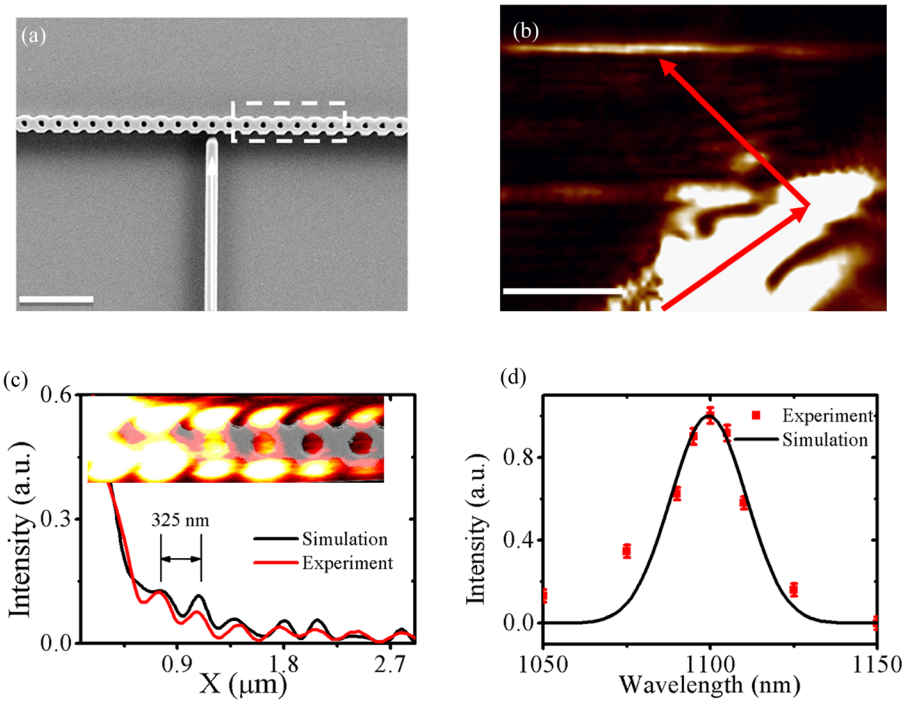

FIG. 1. (a) SEM image of the photonic crystal slab. Scale bar: 1 μm. (b) Near-field intensity distribution of the negative refraction of the photonic crystal. Scale bar: 4 μm. (c) Experimental and simulation result of the lateral profiles of the surface mode of the photonic crystal. Inset: Near-field intensity distribution of the surface mode. (d) Experimental and simulation result of the wavelength dependence of the surface mode intensity.

avoid the strong background from the excitation. The near-field distribution of the surface mode is shown in Fig. 1(c). Periodic peaks locate at the convex region at the surface between the photonic crystal and the air. The separation of the peaks is 325 nm, which is consistent with the designed period on the surface along ΓM direction ($\sqrt{2}$a). The surface mode decays from the excitation source. To confirm the origin of the decay of surface mode, we simulated the surface mode propagation excited by a point source at a wavelength of 1100 nm with different loss value defined as the imaginary part of the complex refractive index of silicon (k) using the finite element method (COMSOL). The propagation length of the experimental result matches well with the simulation result with k = 0.06 as shown in Fig. 1(c). Since this value of k is much larger than that from the absorption of the silicon, this feature might be attributed to the scattering loss due to the imperfect fabrications and the roughness of the sidewall. The intensity of the surface mode peaks at the wavelength of 1100 nm (Fig. 1(d)), which corresponds to a normalized frequency of a/λ = 0.21 and is consistent with the simulation result of the wavelength dependence of the intensity of the surface mode excited by a point source.

The acquired near-field image near the excitation region shows that a focal spot can be found at the output interface (Fig. 2(a)). A lateral FWHM of 350 nm (λ/3) is achieved in the photonic crystal slab with a thickness of a single period, which breaks the theoretical limit of the negative refraction photonic crystal flat lens in the far field (0.36λ).[13] For a comparison, a focal spot of 500 nm (0.45λ) is found in the structure with a thickness of three periods, which can be largely attributed to a reduced coupling strength of surface modes. Fig. 2(b) shows the lateral FWHM of the focal spot as a function of the excitation wavelength. It can be seen that the wavelength for the minimum FWHM is closely related to the resonant excitation of a surface mode for the recovery of the evanescent wave. The FWHM of the focal spot reaches

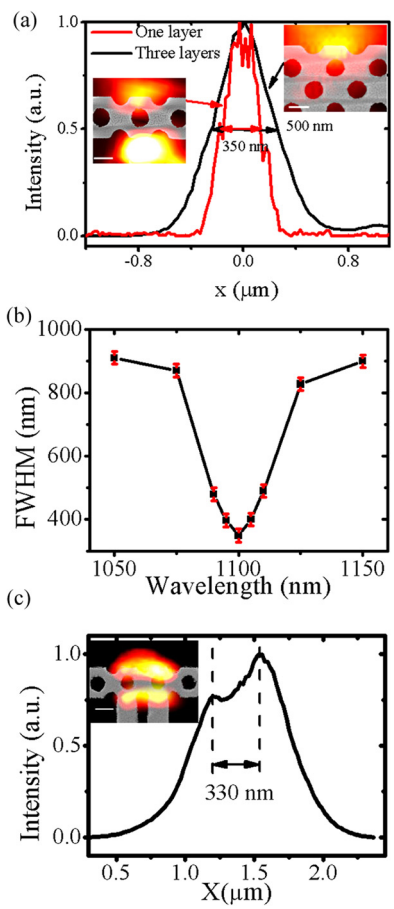

FIG. 2. (a) Lateral profiles of the focal spots of the photonic crystal slab with one and three periods, respectively. Inset: Near-field intensity distributions of the photonic crystal slab with one period and three periods. Scale bars are 200 nm in both insets. (b) Wavelength dependence of FWHM of the photonic crystal slab. (c) Lateral profiles of the focal spot of the photonic crystal slab of two waveguides excitation. Inset: Near-field intensity distribution of the photonic crystal slab with two waveguide excitation. Scale bar: 200 nm.

its minimum at the wavelength of the strongest surface-mode coupling. To confirm the surface-mode enhanced resolution, the excitation with two 200 nm-wide waveguides from the output of a 1×2 splitter that fabricated on the SOI wafer was performed. The output of the two waveguides can be considered as two coherent sources. Indeed, two peaks with a separation of 330 nm can be resolved at 1100 nm (Fig. 2(c)).

To get insight of the surface-mode coupling, we carried out a simulation of the photonic crystal. The negative refraction in the bulk photonic crystal is confirmed by numerically studying the equal frequency contour (EFC) with a plane wave expansion method (Bandsolve, Rsoft). The EFC in TM polarization is shown in Fig. 3(a). Unlike the negative refraction from the negative group velocity,[5] all-angle negative refraction occurs around the normalized frequency of 0.21 in the valence band due to the hyperbolic-like dispersion near the symmetry point M. According to the group velocity equation $vg = \delta\omega/\delta k$, the group velocity always points to M at high normalized frequency. Negative refraction happens if the surface is normal to ΓM direction.[14] The effective refractive index (n_{eff}) of the photonic crystal is calculated by the equation $n_{eff} = \sin(\alpha)/\sin(\beta)$, where α and β are the incident angle and refraction angle, respectively. The refractive index of the photonic crystal at different incident angles is shown in Fig. 3(b). It can be seen that the photonic crystal supports all-angle negative refraction at the normalized frequency of 0.21. The experimental result at an incident angle of 45° in Fig. 1(b) is consistent with the simulation result. (Fig. 3(b)) We studied the dispersion of the surface mode by the supercell method. The dispersion of the surface mode and the bulk Bloch mode projected along the direction of the surface is shown in Fig. 3(b). The surface mode matches with the all-angle negative refraction frequency. The effective refractive index of the surface mode along the surface direction can be calculated by $n_{surface} = k_x/\omega$, where ω is the angular frequency. The dash line in Fig. 3(b) is the light line in the air, which corresponds to a refractive index of 1. The shaded region which stands for the Bloch mode of the photonic crystal is on the left side of the light line. Accordingly, the effective index is restricted to less than 1. The effective refractive index of the surface mode is higher than 1 since it is on the right side of the light line. Therefore, the coupling of surface mode can enrich the high spatial-frequency components for an enhanced resolution. The refractive index of silicon at a wavelength of 1100 nm is 3.545 and the dispersion relation with the wavelength is linear ($dn/d\lambda = -0.467\,\mu m^{-1}$) from 1050 nm to 1150 nm.[15] The refractive index variation due to the dispersion is too small (3.545 ± 0.022) to cause the observed dramatic change in the FWHM. Instead, the dispersion of the photonic crystal mode and the surface mode changes dramatically by a slight shift of the wavelength from 1050 to 1150 nm, which corresponds to the shift of the normalized frequency from 0.22 to 0.20. It can be seen that the photonic crystal can support the all-angle negative refraction and the surface mode at the normalized frequency of 0.21 in Figs. 3(b) and 3(c). Thus, the origin of the FWHM dependence on the wavelength can be attributed to the recovery of the different spatial-frequency components by the all-angle negative refraction and hence the coupling of the surface mode. The negative refraction is responsible for recovering the relative low spatial frequency components of the propagation wave. The surface mode can recover the high spatial frequency components of the evanescent wave. Without the negative refraction, the hot spot can not be formed at the opposite outlet of the photonic crystal slab, which was confirmed by the theoretical analysis.[12] Therefore, the FWHM reaches a minimum when the all-angle negative refraction occurs and the coupling strength of the surface mode peaks at the resonant wavelength. Inset of Fig. 3(c) shows the intensity distribution of the surface mode calculated by the supercell method, which is consistent with the experimental observation of the surface mode in Fig. 1(c).

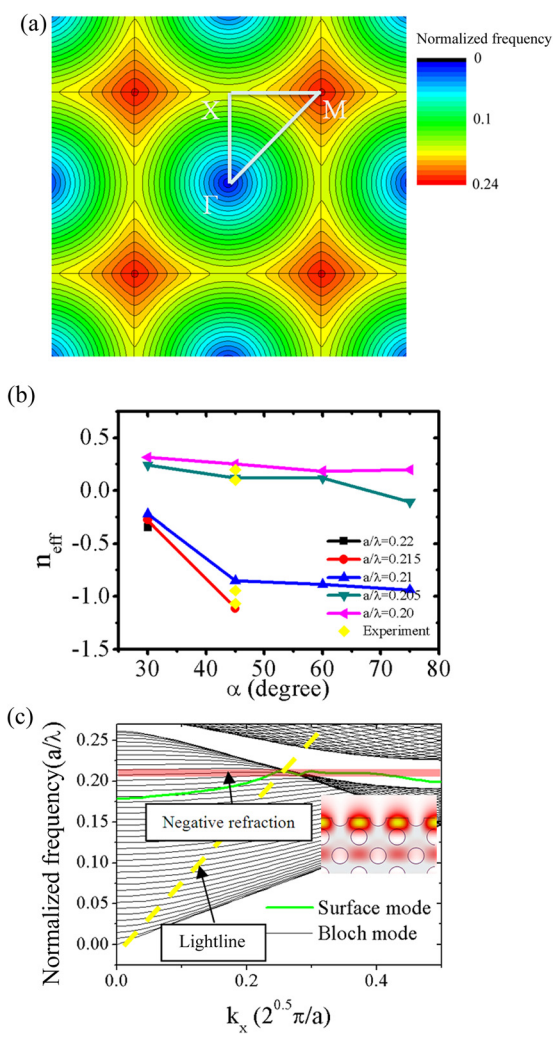

FIG. 3. (a) Equal frequency contour of the photonic crystal at the valence band. (b) Simulation and experimental result of the effective refractive index of the photonic crystal at different incident angle and wavelength. (c) Dispersion of surface modes and the Bloch mode of the photonic crystal projected along the surface direction. Inset: Intensity distribution of surface modes of the photonic crystal.

To verify the surface-mode enhanced nano-imaging, we simulated the focusing by the structure using the finite element method. A point source at the wavelength of 1100 nm is used as the excitation source to test the resolution of the photonic crystal slab. It shows that a focal spot can be formed at the output interface of the photonic crystal slab (Fig. 4(a)). Fig. 4(b) shows the FWHM of the focal spot as a function of the thickness of the photonic crystal. Indeed, the

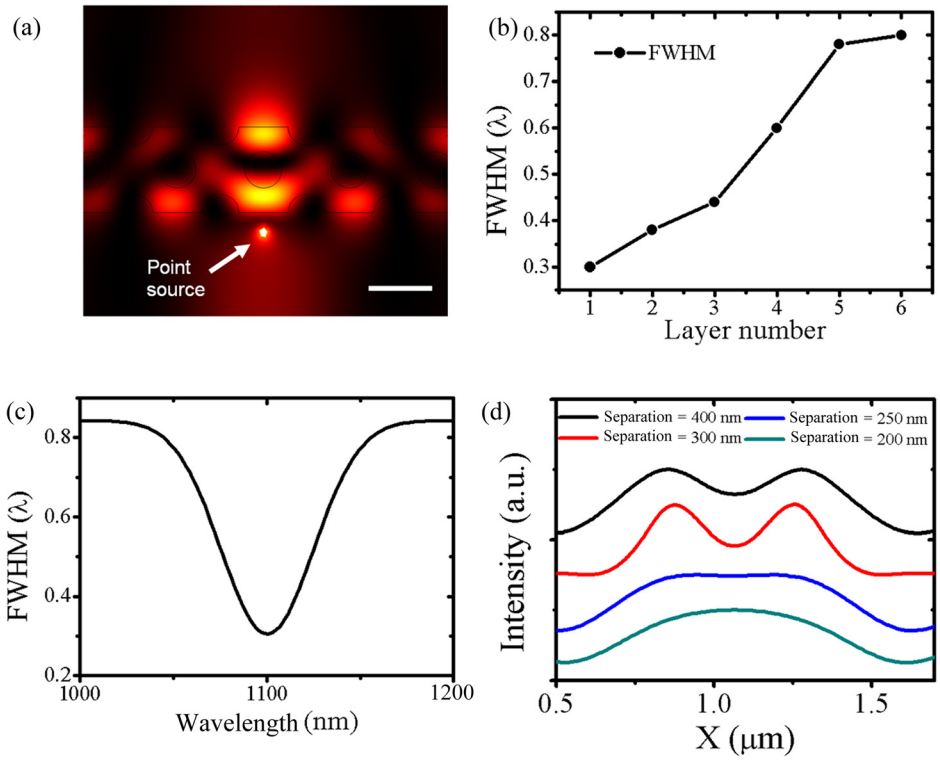

FIG. 4. (a) Simulation result of the photonic crystal slab. Scale bar: 200 nm. (b) Thickness dependence of the lateral FWHM of the focal spot. (c) Wavelength dependence of the lateral FWHM of the focal spot. (d) Simulation of the lateral profiles of the images of the photonic crystal slab with two excitation source with different separation.

resolution improves when the thickness are decreased, which is consistent with the experimental observation. The lateral FWHM reaches its minimum at a wavelength of 1100 nm, which shows strongest coupling of the surface mode (Fig. 4(c)). The simulation result of the two point source excitation with different separations is shown in Fig. 4(d). The evolution of the resolution in different separations of two spots clearly shows that two objects can be resolved when the separation is larger than 250 nm.

The resolution is limited by the coupling strength of the highest spatial-frequency components of the surface mode. This is consistent with the previous theoretical investigation that the resolution (Δ) of the photonic crystal slab can be estimated from equation $\Delta = a_s\lambda/2(\lambda\text{-}a_s)$, where a_s is the surface lattice constant of the photonic crystal.[12] Therefore, the resolution of the photonic crystal slab is limited to $\sim\lambda/4$ based on a surface lattice constant of $\lambda/3$ in our experiment. Thus, an object smaller than $\lambda/4$ cannot be resolved by the photonic crystal slab anymore. Since the spatial resolution depends on the coupling strength of the surface mode, it increases once the separation of the point source with respect to the lens decreases and the wavelength reaches the resonant wavelength of the surface mode. On the contrary, the resolution decreases when the period number of the thickness increases owing to a reduced coupling strength of the surface mode on the outlet surface, as shown in Fig. 4(b).

For a comparison, the spatial resolution of the photonic crystal slab is comparable with the Si immersion microscope, which is $\sim\lambda/5$,[16] and slightly lower than the SNOM, which is $\sim\lambda/10$.[17] On the other hand, the photonic crystal slab has unique advantages in high compactness and parallel imaging.

In conclusion, we have experimentally demonstrated the nano-imaging in a negative refraction photonic crystal slab based on the surface-mode coupling. Our result shows that the surface mode of the photonic crystal can be used to recover the evanescent waves, which allows a loss-less nano-imaging working at the transparent wavelength of dielectric materials rather than the lossy plasmonic resonant wavelength of metals. Near-field scanning optical microscopy confirms the coupling of the surface modes of the silicon photonic crystal and reveals the nano-imaging with a $\lambda/3$ focal spot at the predicted wavelength of 1100 nm. Our result can not only hold the potential of super-resolution imaging but also be useful for compact on-chip optical devices for integrated optics.

This work was supported by the Australian Research Council (ARC) Laureate Fellowship scheme (FL100100099). This work was performed in part at the Melbourne Centre for Nanofabrication. The authors thank Dr. Matteo Altissimo and Dr. Sasikaran Kandasamy of Melbourne Centre for Nanofabrication for the help in fabrication of samples.

[1]J. B. Pendry, Phys. Rev. Lett. **85**(18), 3966–3969 (2000).
[2]V. G. Veselago, Sov. Phys. Usp. **10**(4), 509–514 (1968).
[3]N. Fang, H. Lee, C. Sun, and X. Zhang, Science **308**(5721), 534–537 (2005).
[4]V. A. Podolskiy, N. A. Kuhta, and G. W. Milton, Appl. Phys. Lett. **87**(23), 231113 (2005).
[5]M. Notomi, Opt. Quantum Electron. **34**(1-3), 133–143 (2002).
[6]R. Moussa, S. Foteinopoulou, L. Zhang, G. Tuttle, K. Guven, E. Ozbay, and C. M. Soukoulis, Phys. Rev. B **71**(8), 085106 (2005).
[7]J. B. Chen, Y. Wang, B. H. Jia, T. Geng, X. P. Li, L. Feng, W. Qian, B. M. Liang, X. X. Zhang, M. Gu, and S. L. Zhuang, Nat. Photonics **5**(7), 239–245 (2011).
[8]E. Cubukcu, K. Aydin, E. Ozbay, S. Foteinopoulou, and C. M. Soukoulis, Nature **423**(6940), 604–605 (2003).
[9]P. V. Parimi, W. T. T. Lu, P. Vodo, and S. Sridhar, Nature **426**(6965), 404 (2003).
[10]B. D. F. Casse, W. T. Lu, R. K. Banyal, Y. J. Huang, S. Selvarasah, M. R. Dokmeci, C. H. Perry, and S. Sridhar, Opt. Lett. **34**(13), 1994–1996 (2009).
[11]R. D. Meade, K. D. Brommer, A. M. Rappe, and J. D. Joannopoulos, Phys. Rev. B **44**(19), 10961–10964 (1991).

[12]C. Y. Luo, S. G. Johnson, J. D. Joannopoulos, and J. B. Pendry, Phys. Rev. B **68**(4), 045115 (2003).
[13]C. Y. Li, J. M. Holt, and A. L. Efros, J. Opt. Soc. Am. B **23**(3), 490–497 (2006).
[14]C. Luo, S. G. Johnson, J. D. Joannopoulos, and J. B. Pendry, Phys. Rev. B **65**(20), 201104 (2002).
[15]E. D. Palik, *Handbook of Optical Constants of Solids* (Academic, New York, 1985).
[16]D. A. Fletcher, K. B. Crozier, K. W. Guarini, S. C. Minne, G. S. Kino, C. F. Quate, and K. E. Goodson, J. Microelectromech. Syst. **10**(3), 450–459 (2001).
[17]L. Novotny, D. W. Pohl, and B. Hecht, Opt. Lett. **20**(9), 970–972 (1995).